School of Electronics and Computer Science
University of Southampton

By,

Rajarshi Chakraborty

26th September, 2008

A Low cost Laser Raman Spectrometer for Sample Imaging and Analysis

Project supervisor: Dr. Harold.M.H.Chong
Second examiner: Prof.Dr. Peter Ashburn

A project report submitted for the award of
Master of Science

Abstract:

Traditionally Raman spectroscopy of samples is done by high cost, high-resolution and highly reliable Raman spectrometers. However, an economical lab based Raman spectroscopy system for undergraduates and postgraduates teaching and demonstration is still lacking. There have been introduction of less expensive, portable solid state laser or gas laser excitation sources and the recent availability of rugged, CCD-based modular spectrometers which has motivated the need to produce a low cost, reliable and compact Raman spectroscopy system based on optical bench-top set-up. This miniaturized laboratory bench-top spectrometer can be used for on-site, in situ, real-time monitoring and offer rapid and non-destructive qualitative and quantitative of many analytes often with little or no sample preparation.

Performance of the instrument is demonstrated on *Isopropyl Alcohol* ($(CH_3)_2CHOH$), *Klarite 307 SERS substrate coated with organic materials with Thiophenol* (C_6H_5SH) substance presence *and commercial grade Paracetamol* ($C_8H_9NO_2$). These experiments show Stokes radiation bands in agreement with published data. While for using long wave pass filters and dichoric mirror assembly and also for the limited optical resolution of the modular CCD spectrometer have obscured some Raman vibrational bands, the instrument serves to illustrate fundamental principles of Raman spectroscopy appropriate for physical sciences or chemistry teaching laboratories.

Table of Contents

List of Figures:

Acknowledgements

I would like to thank my supervisors, Dr.Harold.M.H.Chong and Dr. Peter Ashburn for their invaluable support, guidance and patience. I would also like to express gratitude especially to Dr.Harold for his effort in implementing the setup and for always lending a helpful hand in general.

I would also like to thank Nanoscience Research Group, University of Southampton for funding several components for the setup assembly under supervision of Dr.Harold.M.H.Chong.

1. Introduction:

Raman spectroscopy is a form analytical technique of investigating the rotational and vibrational frequency modal characteristics of material. It is similar to IR Infrared spectroscopy in many aspects except that IR bands arise from a change in the dipole moment in the molecule whereas Raman bands arise from a change in polarizability of the molecules. Raman spectroscopy has gained popularity because it allows rapid, non-destructive qualitative or quantitative analysis of many sample types with little or no sample preparation requirements [1]. In this project I have realised a low cost Raman spectrometer with a He-Ne 633 nm gas laser source as excitation source, coupled to a polariser and a quarter wave-plate, a laser line filter or excitation band–pass filter for the source, a longwave pass filter as Rayleigh scattering filter, a dichroic mirror to reflect light of the wavelength of the laser and to allow Raman scattering to pass through it [2-3]. The dichoric mirror mount was used in my Raman system between the excitation and barrier filters at an angle of 45 degrees, to direct the laser beam to the sample. For low Raman scatterers a T300-RT UV/VIS optical fibre probe with collection optics have been used i.e. collecting and directing the laser towards the sample. At the end the collected invisible Raman scattering is analysed by a commercial Ocean Optics broadband high-res CCD-based miniature modular spectrometer [HR-4000]. In addition, this Raman spectrometer has the potential to use for biochemical sensing application and also couple to an Atomic Force microscope to ensure a complete sample imaging and spectroscopic analysis.

2. Background:

2.1 The Raman Effect and Normal Raman Scattering:

When incident light is scattered from a molecule most photons are elastically scattered. The elastically scattered photons have same energy (frequency) and wavelength as the incident photons. However, a small fraction of light (1 in 10^7 photons approx.)[4] is scattered at frequencies different from and usually lower than the frequencies of the incident photons. This process of inelastic scattering of incident photons is termed as Raman Effect [5], named after the discoverer Dr. C.V. Raman in 1922. Dr. Raman received the Nobel Prize in 1930 for his work on the scattering of light. In recognition of Raman Effect's significance as a tool for analysing the composition of liquids, gases and solids, it was designated an ACS [American Chemical Society] National Historical Chemical Landmark in 1998 [6].

Now as explained before if a liquid, solid or gaseous sample is irradiated with a beam of monochromatic light, such as in our case 632.8 nm He-Ne Laser , light will be scattered which has an intensity component ν_L with the same frequency as the incident Laser radiation and weak components at pairs of frequencies $\nu_{L\pm}\nu_M$. Here ν_M usually has a value associated with rotational or vibrational energy level changes. If the incident radiation lies in the visible spectrum, for vibrational energy changes these frequency shifts are typically ≈ 1% of the

frequency of the incident radiation and the intensity of one of these frequency shifted lines is typically ≈ 10^{-6} × incident radiation intensity [7]. Measuring these frequency shifts along with the polarisation and direction dependence of the intensity of the scattered radiation provide information on the energy states and molecular structure of the irradiated sample. This as a spectroscopic technique is widely used in research and in routine spectroscopic measurements where the result may be used to support and in many cases complement, infrared spectroscopic results. A plot of intensity of scattered light versus these frequency shifts is a Raman Spectrum.

2.1.1 Scattering Process:

Raman effect arises when an incident photon on a molecule interacts with the electric dipole of the molecule. It is a form of electronic (more accurately, vibronic) spectroscopy, although the spectrum contains vibrational frequencies. Classically, the interaction can be viewed as a perturbation of the molecule's own electric field. In quantum mechanics the scattering is described as an excitation to a virtual state lower in energy than a real electronic transition with nearly coincident de-excitation and a change in vibrational energy. The scattering event occurs in 10^{-14} seconds or less. The virtual state description of scattering is shown in figure-1.

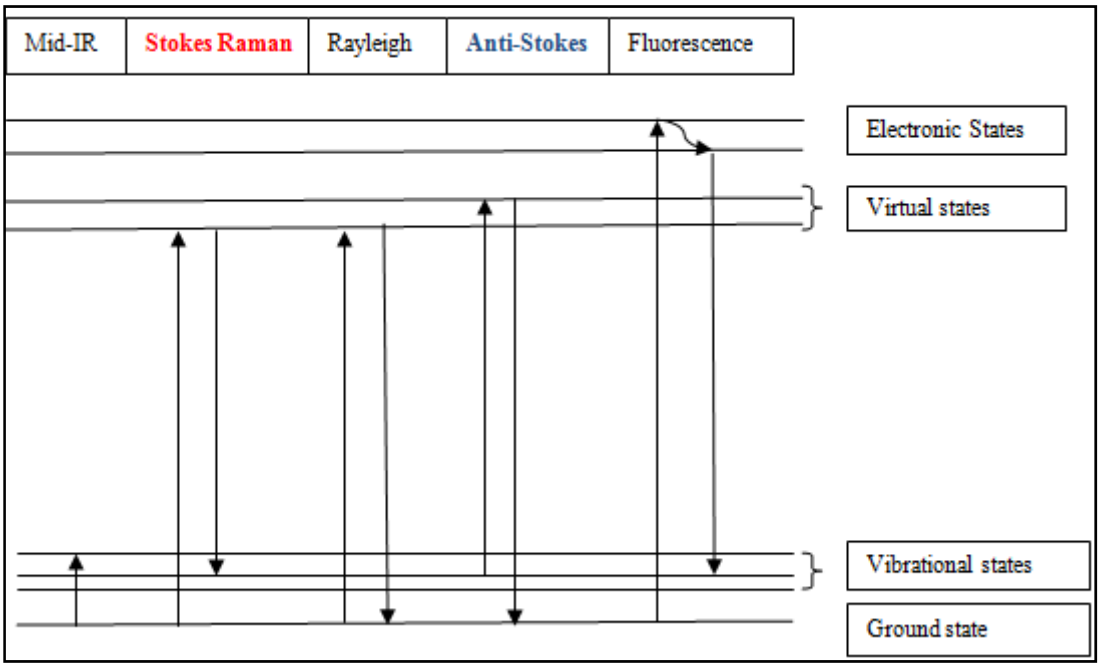

Figure 1: Jablonksi energy diagram representation of Raman shifts with stokes and anti-stokes lines redrawn from ref [8]

The difference in energy between the incident and scattered photons is represented by the different lengths of arrows in the above Jablonksi energy diagram fig-1. Numerically, the energy difference between the initial and final vibrational levels, ύ, or Raman shift in wave numbers (cm^{-1}), is calculated by equation-1

$$ύ = 1/\lambda_{incident} - 1/\lambda_{scattered} \qquad (1)$$

.where $\lambda_{incident}$ and $\lambda_{scattered}$ are the wavelengths (cm^{-1}) of the incident and Raman scattered photons, respectively. And the strength of Raman signal is given by [9],

$$R \propto I_{Laser} \times (\nu_{Laser} - \nu_{Raman})^4 \times b^2 \times a_\gamma \times g$$

Where b, aγ and g are constants depending upon specific molecular properties. The vibrational energy is dissipated as heat. But because of the low intensity of Raman scattering, the heat dissipation does not cause a measurable temperature rise in the sample. In Rayleigh scattering the electron decays back to the same level from where it started as seen in the fig-1. In Stokes and anti-stokes both types of Raman scattering the electron decays to a different level than that where it started. Stokes Raman scattering happens when the final energy level is higher than the initial level, while anti-Stokes Raman scattering occurs when the final energy level is lower than the starting level. According to Boltzmann distribution at any given time an electron in the most common temperature range is most likely to be in its lowest energy state, so Stokes scattering is much more common than anti-Stokes scattering. Only Stokes Raman scattering is commonly used in spectroscopy.

The anti-Stokes-shifted Raman spectrum is always weaker than Stokes-shifted spectrum as explained before, but at room temperature it is strong enough to be useful for vibrational frequencies less than about 1500 cm^{-1}. The Stokes and anti-stokes spectra contains the same frequency information. The ratio of anti-stokes to stokes intensity at any vibrational frequency gives measure of temperature. Anti-Stokes Raman scattering is used for contact less thermometry and it is also used when Stokes spectrum is not directly observable due to poor detector response or spectrograph efficiency [10].

2.1.2 Vibrational Energies:

The vibrational mode energy depends on molecular structure and symmetries and ambient conditions. Atomic mass, bond order, molecular substituents, molecular geometry and hydrogen bonding all affect the vibrational force constant and in turn dictate the vibrational energy. As for example the stretching frequency of a phosphorous-phosphorous bond ranges from 460 to 610 to 775 cm^{-1} for the single, double and triple bonded species, respectively [11]. Much effort has been given into the estimation and measurement of force constants. For small molecules and even for some extended structures such as peptides, moderately accurate calculations of vibrational frequencies are possible by commercially available softwares. Vibrational Raman spectroscopy is not only limited to intramolecular vibrations, but also crystal lattice vibrations and other motions of extended solids are Raman-active. Their spectra are important in such fields as polymers and semiconductors. In the gas phase rotational structure is resolvable through vibrational transitions and the resulting vibrational/rotational spectra are widely used to study flame species and gas phase reactions generally. Vibrational Raman spectroscopy in this broad sense is an extraordinarily versatile probe into a wide range of phenomena ranging across disciplines from physical biochemistry to material science [12].

2.1.3 Raman Selection Rules and Intensities according to classical theory:

Many of the important features of Raman band intensities can be explained by a simple classical electromagnetic field description of Raman spectroscopy. The dipole moment, **P**, induced by an external electric field, **E** is proportional to the field as shown in equation 2.

$$\mathbf{P} = \alpha\,\mathbf{E} \qquad (2)$$

The proportionality constant α is called the polarizability of the molecule. The polarizability defines the ease of distortion of the electron cloud around a molecule if an external electric field is applied. The induced dipole primarily emits or scatters light at the same optical frequency of the incident light wave. Raman scattering occurs because a molecular vibration can change polarizability of the molecule. This change is generally defined by polarizability derivative, $\frac{\partial\alpha}{\partial Q}$, where Q is the normal coordinate of vibration. The selection rule for Raman-active vibration, that there is a change in polarizability during the vibration is given by the equation-3

$$\frac{\partial\alpha}{\partial Q} \neq 0 \qquad (3)$$

Scattering intensity is proportional to the square of induced dipole moment that is to the square of the polarizability derivative [13], $\left(\frac{\partial\alpha}{\partial Q}\right)^2$.

When a sample of a molecule whose polarizability is non-zero is subjected to a beam of radiation of frequency ν, the electric field experienced by each molecule varies according to the equation,

$$E = E_0 Sin2\pi\nu t \qquad (4)$$

And thus induced dipole also undergoes collisions of frequency ν:

$$U = \alpha\, E = \alpha\, E_0 sin2\pi\nu t \qquad (5)$$

This oscillating dipole emits radiation of its own oscillation frequency. If the molecule undergoes vibrational or rotational motion which in effect changes its polarizability periodically, then the oscillating dipole will have superimposed upon it the vibrational or rotational collision. Considering a vibration of frequency ν_{vib} which changes polarizability: we can write, $$\alpha = \alpha_0 + \beta sin2\pi\nu_{vib}t \qquad (6)$$

Where α_0 is the equilibrium polarizability and β represents the rate of change of polarizability with the vibration. Then we have:

$$U = \alpha_E = (\alpha_0 + \beta sin2\pi\nu_{vib}t)E_0 sin2\pi\nu t \qquad (7)$$

Or expanding and using the trigonometric relation:

$$2sin\ A \sin B = \{\cos(A-B) - Cos(A+B)\}$$

We have [14], $U = \alpha_0 E_0 sin2\pi\nu t + \frac{1}{2}\beta E_0\{cos2\pi(\nu - \nu_{vib})t - cos2\pi(\nu + \nu_{vib})t$

And it can be seen that resulting equation that the oscillating dipole has frequency components $\nu \pm \nu_{vib}$ as well as the exciting frequency ν.

If a vibration does not greatly change the polarizability, then clearly the polarizability derivative will be nearly zero and the intensity of the Raman band will be low. In case of highly polar moieties, such as the O-H bond the vibrations are usually weak. An external electric field can not induce a large change in the dipole moment of such polar and symmetric molecular bonds. Typical strong Raman scatterers are moieties with distributed electron clouds, such as carbon-carbon double bonds. The pi-electron cloud of thee double bond is easily distorted in an external electric field which bends or stretches the bond which changes the distribution of electron density substantially, and causes large change in induced dipole moment[14].

The quantum-mechanical approach to Raman scattering theory relates scattering frequencies to intensities of vibrational and electronic energy states of the molecule. The standard perturbation theory assumes the frequency of the incident light is low compared to the frequency of the first electronic excited state. The small changes in the ground state wave function are defined by the sum of all possible excited vibronic states of the molecule.

2.1.4 Quantum Theory of Raman Effect:

The quantum theory of radiation helps understand the occurrence of raman scattering perhaps most easily. This treats radiation of frequency ν as consisting a stream of particles (photons) having energy hν where h is the planck's constant. Photons can be depicted to undergo collisions with molecules and if the collision is perfectly elastic they will be deflected with unchanged energy level. However it can happen that energy is exchanged between photon and molecule during the collision: which is by nature inelastic. The molecule can gain or lose amounts of energy only in accordance with the quantal laws; i.e. ΔE joules must be the difference in energy between two of the allowed states. ΔE represents a change in vibrational or rotational energies of the molecule. If the molecule gains energy ΔE in the inelastic collision with the incoming photon, the photon will be scattered will be scattered with energy hν-ΔE and the equivalent radiation will have a frequency ν-ΔE/h. Conversely if the molecule loses energy ΔE, the scattered frequency will be ν+ΔE/h. Radiation scattered with a frequency lower than that of the incident beam is referred to as Stokes' radiation, while the radiation at higher frequency is called ant-Stokes' radiation [14]. Now as explained before, according to Boltzmann distribution at any given time an electron in the most common temperature range is most likely to be in its lowest energy state, the stokes radiation,

accompanied by an increase in molecular energy is more intense than anti-stokes radiation (decrease in molecular energy) which can only occur if the molecule is originally in an excited vibrational or rotational excited state. Overall the total radiation scattered at any but the incident frequency (Rayleigh scattering) is extremely small and sensitive apparatus is needed for its study.

2.1.5 Polarization Effects:

For molecules in a gas or liquid, Raman scatter is partially polarized even when the individual molecules are randomly oriented in a gas or liquid. This effect is clear to be seen if the excitation source is plane polarized. In isotropic media polarization arises because the induced electric dipole has spatially varying components with respect to the coordinates of the molecule. For totally symmetric vibration Raman scatter will be strongly polarized parallel to the plane of polarization of the incident light. In case non-symmetric vibrations the scattered light intensity is only $3/4^{th}$ as strong in the plane perpendicular to the plane of polarization of the incident excitation light as in the plane parallel to it [15].

In crystalline material the orientation of the crystal is fixed in the optical system. The polarization components depend on the orientation of the crystal axis with respect to the plane of polarization of the input light as well as on the relative polarization of the input and the observing polarizer.

2.2 Surface Enhanced Raman Scattering:

The Raman scattering from a compound or ion adsorbed on or even within a few nanometers of a structured metal surface can be significantly higher (10^3-10^6 times greater) than even concentrated or saturated solution. SERS Raman scattering is strongest on silver though gold, copper, platinum also displays same properties. SERS from Pyridine adsorbed in the electrochemically roughened silver was first observed by Dr. Martin Fleishman of University of Southampton and co-workers in 1974 [16]. The exact mechanism behind this signal enhancement effect of metal nanoparticles is still under debate in literature. In 1977 two individual research groups proposed separate mechanisms to explain the observed enhancement which still constitute the underlying principals for modern SERS effect theories. Jean Marie and Van Duyne proposed an electromagnetic effect [17], while Albrecht and Creighton proposed a chemical charge-transfer effect [18].

The electromagnetic theory depends on excitation of localized surface plasmons and the chemical theory rationalizes the effect through the formation of charge-transfer complexes which only applies to species that have formed a bond with the surface. On the contrary the electromagnetic theory can be applied to even those cases where the specimen is only physisorbed in the surface.

Electromagnetic theory says that when the incident excitation light wavelength is close to the plasma wavelength of the metal, conductions electrons in the metal surface are excited into

an extended surface electronic excited state called a surface plasmon resonance. Molecules adsorbed or in a few nanometers of the surface experience an exceptionally large electromagnetic field. As a result vibrational modes normal to the surface are most strongly enhanced.

Electromagnetic theory on the other hand cannot fully explain the magnitude of the enhancement observed in many systems. For many molecules consisting lone pair of electrons, in which the molecules bond to the surface a different mechanism involving charge transfer between the chemisorbed species and the metal surface. This chemical mechanism probably occurs in concert with the electromagnetic mechanism.

Molecules with lone pair of electrons or pi-clouds display the strongest SERS effect [19]. Aromatic nitrogen or oxygen containing compounds such as aromatic amines or phenols are strongly SERS active. The intensity of the surface plasmon resonance is dependent on many factors including the wavelength of the incident light and the morphology of the metal surface. The wavelength of the incident excitation should be in resonance with the surface plasmon frequency. As for example this is about 382 nm for a 5 μm silver particle [20], but can be as high as 600 nm for larger ellipsoidal silver particles [21]. The plasmon frequency is to the red of 650 nm for copper and gold, the other two metals that show SERS at wavelengths in the 300-1000 nm region.

SERS is used to study monolayers of materials adsorbed on metals, including electrodes. Many formats other than electrodes can be used. Colloids, meta films on dielectric substrates and arrays of metal particles bound to metal or dielectric colloids through short linkages are the most popular of analytes.

2.3 Resonance –Enhanced Raman Scattering:

Raman spectroscopy is conventionally performed with VIS/NIR Lasers. As assumed by scattering theory the wavelengths of these Lasers are below the first electronic transitions of most molecules. If the wavelength of the exciting laser is within the electronic spectrum of a molecule this situation changes significantly in which case the intensity of some Raman-active vibrations increases by a factor of 10^2-10^4. This is called as Resonance enhancement or Resonance Raman effect and can be quite useful in low concentration sample analysis [22]. Several classes of biologically important molecules like metalloporphyrins, carotenoids have strong allowed electronic transitions in the visible. Distinct spectrum of chromophoric moiety is resonance enhanced while that of the surrounding matrix is not which allows researchers to probe the chromophoric site (often active) without significant spectral interference from the surrounding protein matrix. Resonance raman is also a major probe of the chemistry of the fullerenes, polydiacetylenes and other "exotic' molecules which tend to strongly absorb in the visible spectrum. Many molecules tend to absorb in ultraviolet but high cost of UV lasers and

related optics for this spectral region limited the use of UV Resonance Raman spectroscopy to extremely specialized analysis.

The most common vibronic mechanism behind resonance enhanced raman bands is Franck-Condon enhancement [23], in which a component of normal coordinate of vibration is in a direction in which the molecule expands during an electronic excitation. The more the expansion of the molecule along its axis upon absorbing light, the larger the enhancement factor. Vibrations which couple two electronic excited states are also resonance enhanced. This mechanism is called vibronic enhancement. Resonance enhancement does not begin at a sharply defined wavelength. In fact enhancement of 5-10 times is commonly observed if the exciting laser is even within a few hundred wavenumbers below the electronic transition of a molecule [24]. This pre-enhancement resonance was successfully used in our setup with the Klarite 307 SERS substrate displaying SERRS (Surface Enhanced Resonance Raman spectroscopy) effect.

3. Application of Raman Spectroscopy:

Raman mapping, microscopy and spectroscopy provide varied and important information on many sample types; from semiconductors to drugs, polymers to minerals. Chemical composition, bonding, structure, phase, localization, size, induced stress and reaction mechanisms can all be studied with modern raman instruments [25].

4. Previous Work:

The main problems in implementing Raman spectroscopy is cost. Traditionally this technique would require a grating monochromator, photomultiplier tube detector and an intense monochromatic light source. This suggests that Lasers of at least moderate power are the only viable and practical radiation sources. In a low cost approach, several teachers have suggested “dry lab” experiments in which the student interprets reference spectra [26], but this lacks the hands on aspect of performing and assembling setups for an actual experiment. To address this issue, DeGraff et. al [27] assembled an inexpensive Laser raman spectrometer by combining a PC-based spectrometer with a 10mW, 532 nm frequency doubled Nd:YAG laser. Vickers et al [28] have also used a CCD based spectrometer with a very high power (500 mW) 785 nm near-infrared diode laser.

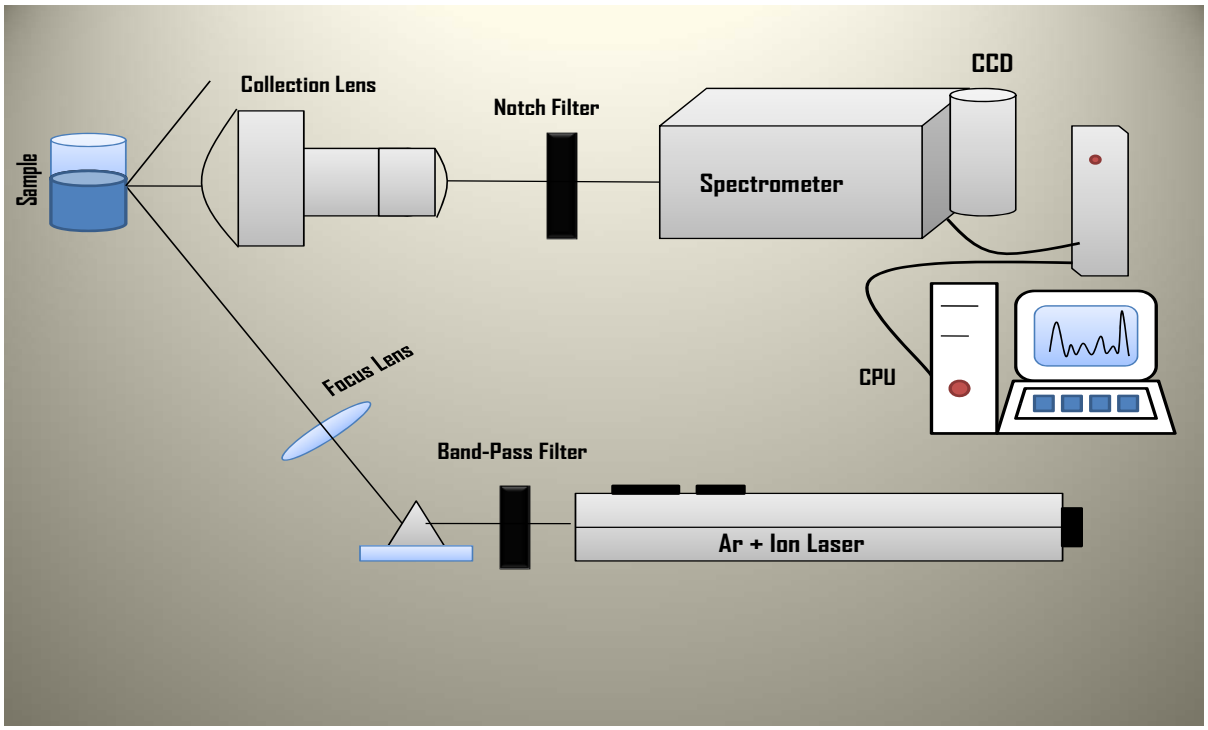

Figure 2: Conventional and commercial Raman spectrometer setup

Because Raman scattering intensity depends inversely on the incident radiation wavelength raised to fourth power , using a shorter wavelength laser could potentially increase the Raman scattering and can reduce the need for higher radiant power. Continuous-wave gas lasers operating in the violet spectral region (400 nm) can be purchased but are costly. On the contrary, red HeNe laser (632.8 nm) has been commercially available for about twenty years and it retains the cost advantage and ease of operation which has made red HeNe laser a favourite in teaching laboratories. As we have already a Thorlabs HRP050, 632.8 nm, 5 mW, polarized He-Ne Laser available at the NSI laboratory, University of Southampton; this propelled me to use this as the excitation source for the Laser raman spectrometer. Raman spectroscopy is rarely explored in teaching laboratories, largely because of the belief that expensive equipment will be required and signal will be too low too detect. However, dispelling the myth, here we present the raman spectra of Klarite SERS substrate coated with thiophenol along with some neat organic liquids that were obtained using a 5 mW red HeNe laser as the excitation source.

5. Instrument Description:

The experimental layout is shown in fig-2; the entire assembly is constructed on a 5 ft by 4 ft steel optical bench from Thor labs. By combining the optical bench with lens holders, base plates and other mounting hardware available from the same vendor, a wide range of suitable configurations are possible that include additional collection and retro mirrors, filters and polarizing filters and polarizing optics.

The components used are a Thorlabs HRP050, 632.8 nm, 5 mW, polarized He-Ne Laser, a 632.8 nm laser line filter LL01-633-25 (25.0 mm) from Semrock, a filter wheel mount with FW1AND and FW2AND neutral density filter assembly, two linear polarizing fiter and a

quarter wave plate with rotational mounts from Thorlabs, a 45^0 50/50 beam splitter from Semrock, a single edge 45^0 laser dichroic mirror (Di01-R635) with reflection band 632.8 nm-647.1 nm and pass band 663.3 nm- 850 nm, a sample holder base from Thorlabs, a 20x objective for focussing purposes, a 25 mm edge based long wave pass filter, a pc based ocean optics modular CCD spectrometer HR 4000 with fibre optics input, a PAX 5710 VIS polarimeter with external sensor head (400nm-700nm) from Thorlabs, several economy front surface mirrors for directional and alignment purposes, an ocean optics TP-300 VIS/NIR transmission probe, a 300 μm diameter fibre optic cable as collection optics and several rotational and kinematic mounts, base plates, 50mm/75 mm posts and post holders.

5.1 Excitation Source: The He-Ne 632.8 nm laser (shown in fig- 3) was used as the excitation source in the assembly.

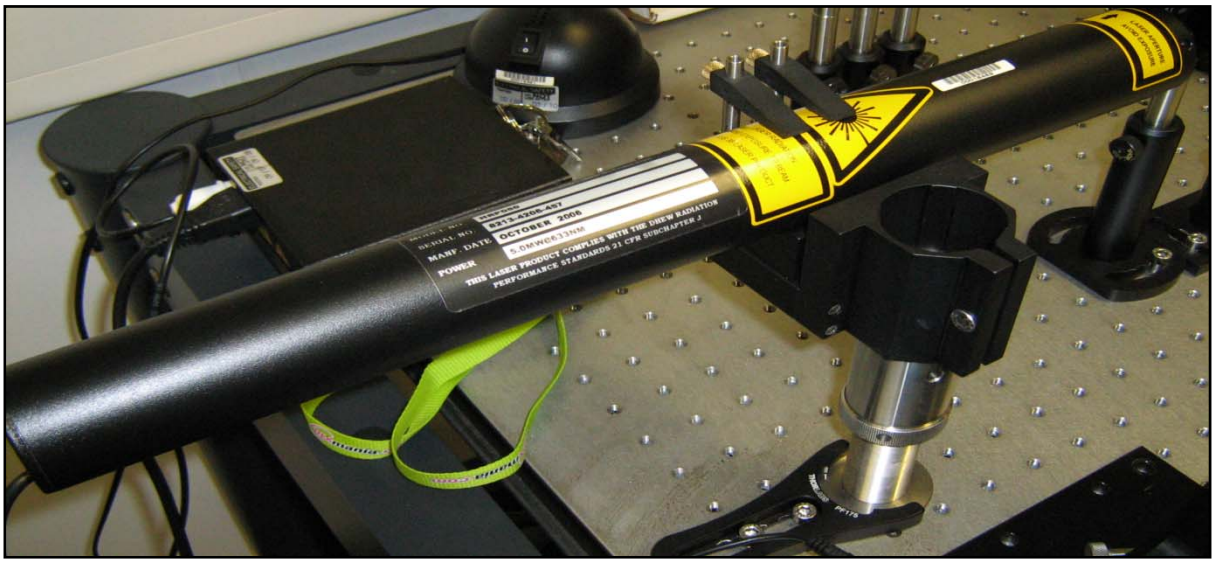

Figure 3: Excitation source 632.8 nm, 5 mW He-Ne laser used in our setup

This low power laser exhibit outstanding stability and performance. This tube design features four holes located in front for easy mounting of accessories. It comes with a separate switchable power supply with locking mechanism for security purposes. Operating range of the laser lies from -20^o to 70^o Celsius though the experiment was done on controlled 20^o Celsius. The laser is linearly polarized with azimuth angle 72^o (measured with polarimeter) with 500:1 extinction ratio. A convenient actuator shutter was also present in the laser assembly [29]. But the laser source was generating a secondary wavelength at 640 nm with intensity less than 2000 counts (shown in fig-4). Several steps was taken to remove this erroneous wavelength, as for example laser warming up time is increased to upto 1 hour but it did not effect the output of the laser line, then using a 632.8 nm laser line filter was given a thought and employed successfully resulting in a clean laser line.

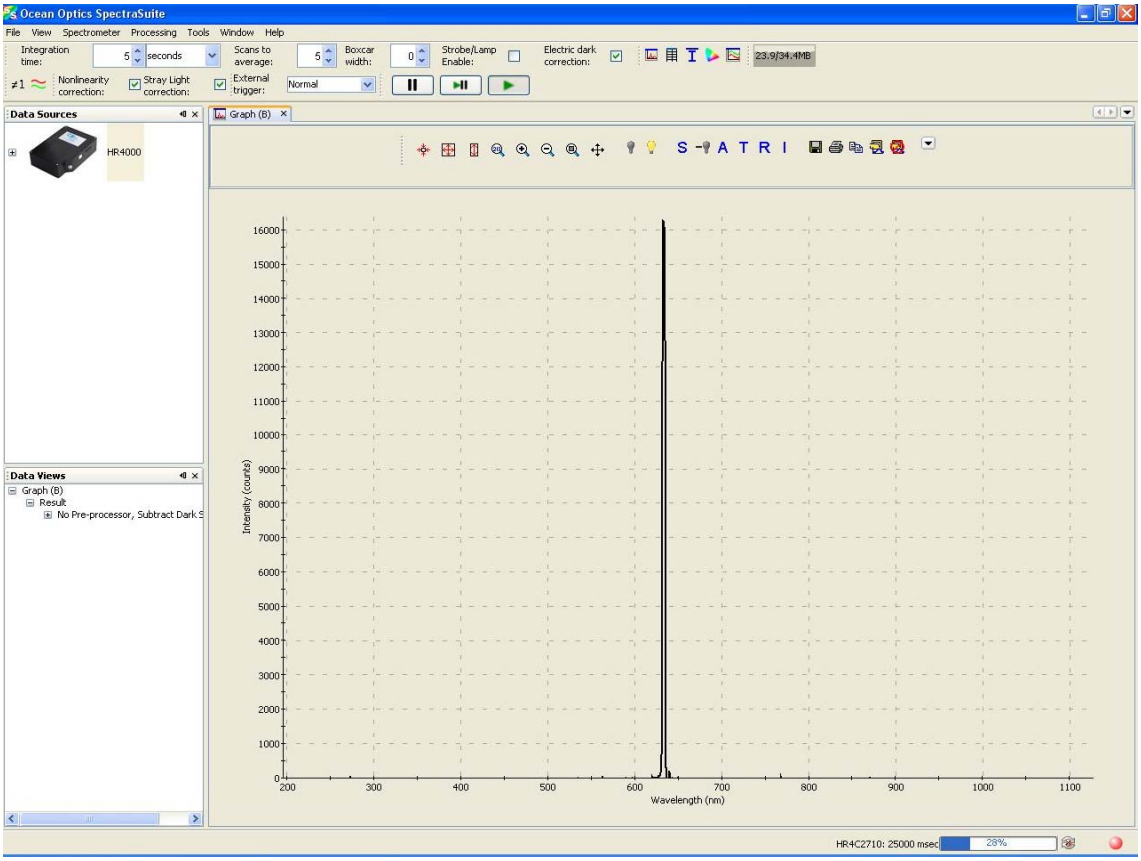

Figure 4: Laser line spectra as seen on Spectrasuite software bundled with HR-4000 spectromter

Figure 5: Neutral density filter wheel assemblies redrawn from ref [30]

Figure 6: Laser power meter from Thorlabs

5.2 Neutral Density Filter: The FW1AND and FW2AND filter wheel assemblies are convenient lab table organizers along with a set of absorptive neutral density (ND) filters of increasing attenuation. A precision mechanical indexer provides precise alignment and

positional holding force for repeatability. It is used here to reduce or block the high power laser into reaching the specimen.

Calculation of Optical Density (OD):

It is documented in the catalogue [30] for Neutral density filter assembly at the Thorlabs portal that $OD = \log_{10}(1/T)$ or $T = 10^{-OD}$; where T = Transmission.

However I conducted a small set of experiment to record the accuracy of the logarithmic relation between transmission and optical density with a Thorlabs Laser power meter, 632.8 nm He-Ne laser and FW1AND and FW2AND filter wheel assemblies with neutral density filters. The experiment corroborated the documented relation perfectly. Below is the table for transmitted power vs ND filters. And fig-6 shows the scatter chart between these two variables which is perfectly logarithmic.

Neutral Density	Transmission intensity
0.6	0.25
1.0	0.1
2.0	0.01
3.0	0.001

Table 1 : Neutral Density vs Transmission efficiency chart

With laser power meter this calculation was corroborated as for we have taken measurements of the output laser power from the neutral density filter by a laser power meter by Thorlabs.

Table 2: Transmission efficiency vs Power output by laser power meter

Transmission	Power o/p by laser power meter
0.25	1.215 mW
0.1	500µW
0.01	60 µW
0.001	12 µW

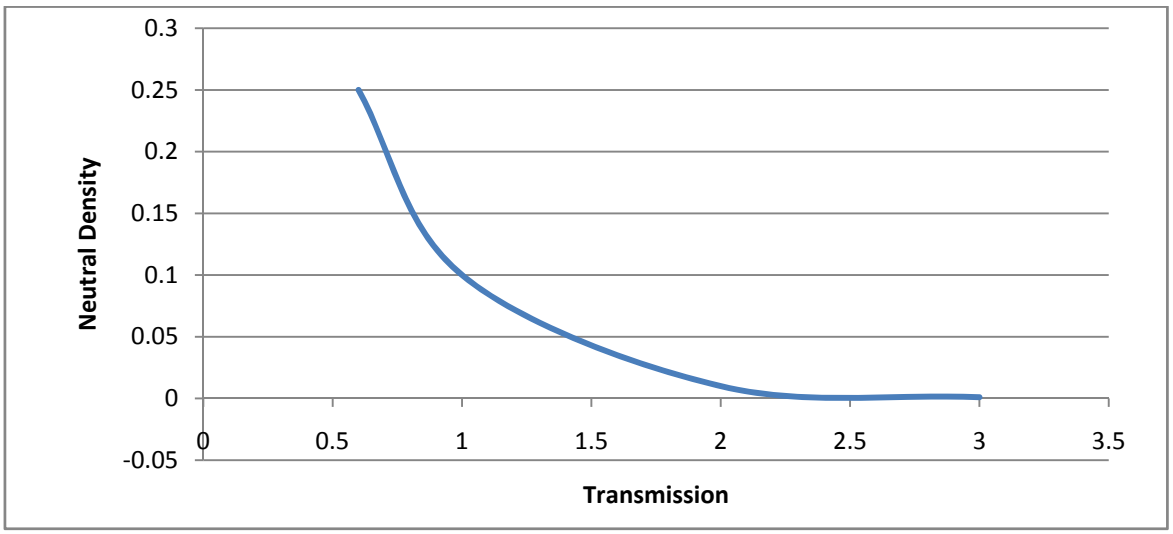

Figure 7: Transmission vs Neutral density curve

When combining two ND filters in series, the ND filter values are additive. So if a ND 0.2 filter was placed in front of an ND 3.0 filter, the total ND of the optical assembly would be 3.2, effectively attenuating the intensity of the input beam by $10^{3.2}$. By combining 10 absorptive Neutral Density filters into a two wheel assembly, optical assemblies can be changed over a large dynamic range (1 to 10^8). The ND filter values for each filter wheel are described below:

- FW1AND includes: 0.5, 1, 2, 3, 4 Absorptive Optical Density Filters
- FW2AND includes: 0.2, 0.3, 0.4, 0.5, 0.6, 1, 2, 3, (2) 4 Absorptive Optical Density Filters

However in our case we have only used FW1AND filter assembly and 2.0 ND filter which suffices our need to reduce the transmission to 50 µW from 5 mW.

Figure 8: Two linear Polarizer and a quarter wave plate lined up as polarizer-analyser setup

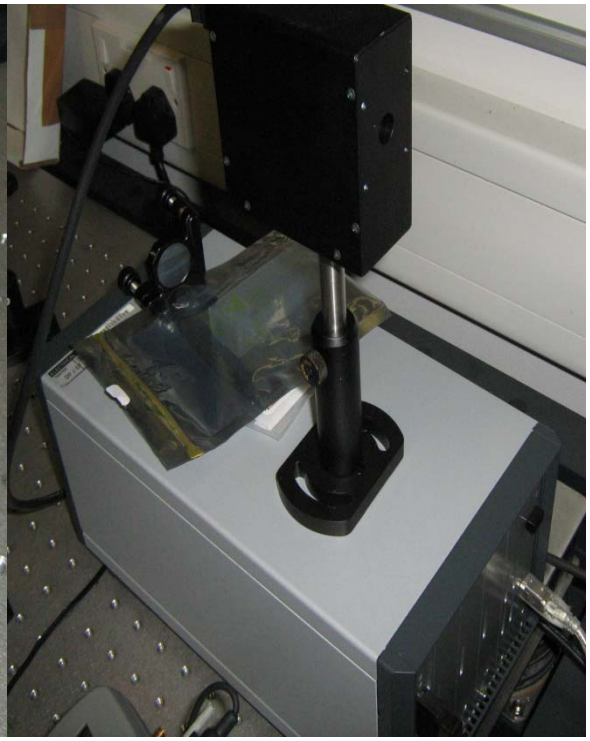

Figure 9: PAX 5710 VIS/NIR polarimeter with sensor head

5.3 Polarizing filter assembly:

Two linear polarizing filters and a quarter wave plate (shown in fig -7)was used to make the 72^o azimuth linearly polarized He-Ne laser output, perfectly horizontally polarised; and also to measure the depolarization ratio quantitatively and to further the experiment for observing the effect of different polarization of the excitation laser on the Raman shifts of different sample. To perfectly control the polarisation of the incident radiation we have used a PAX

5710 VIS polarimeter from Thorlabs with an external sensor head. Another PC was connected with the polarimeter to monitor the polarization point on the Poincare' sphere representation. A scope view of the polarisation of incident radiation was also available from the bundled software TXP monitor which comes with the polarimeter (shown in fig- 8).

Poincare' Sphere Representation:

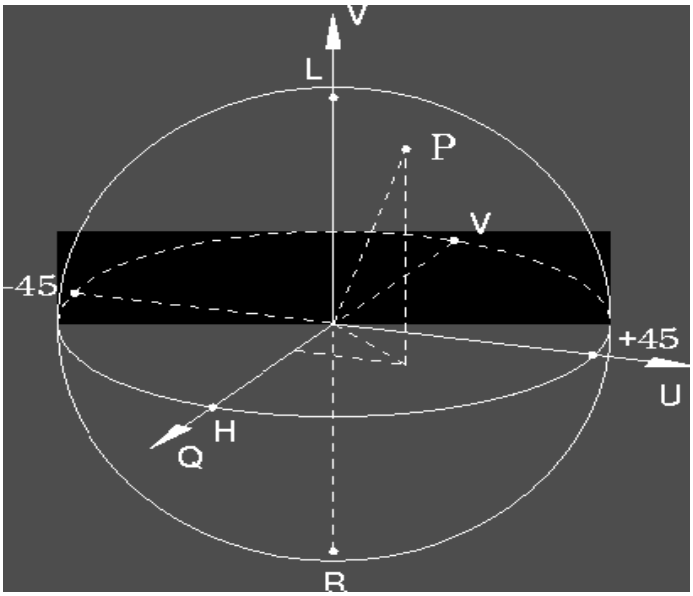

Figure 10: Poincare' Sphere representation of polarization state of light-redrawn from ref [31]

A three dimensional view of Poincare' sphere is depicted in the fig-9. The Parameters Q, U, V constitutes the Cartesian coordinates of the polarization state are Stokes parameters and represented by a point on the surface of the sphere (Scott, 1999). The vertical axis through the centre of the sphere represented by stokes parameter V indicate circular polarization of which L represents left hand circular and R represents right hand circular polarization. The parameter H represents the horizontal linear polarization axis with 0^o azimuth and V represents vertically linear polarization with 90^o azimuth. The x-coordinate of the point, Q, corresponds to the differences of the signal powers measured in an orthogonal H-V basis. Thus $Q= W_H-W_V$. Y and Z coordinate stokes parameters corresponds to $U=2\ |W|\cos\varphi$ and $V = 2|W|\ \cos\varphi$, where $|w|$ and φ are the magnitude and phase of H-V cross covariance(Krehbiel and Scott, 1999). The radius of the Poincare' sphere corresponds to the power of the polarized part of the signal, $I_P = \sqrt{(Q^2+U^2+V^2)}$. A signal point at H parameter in the sphere would therefore have all its power

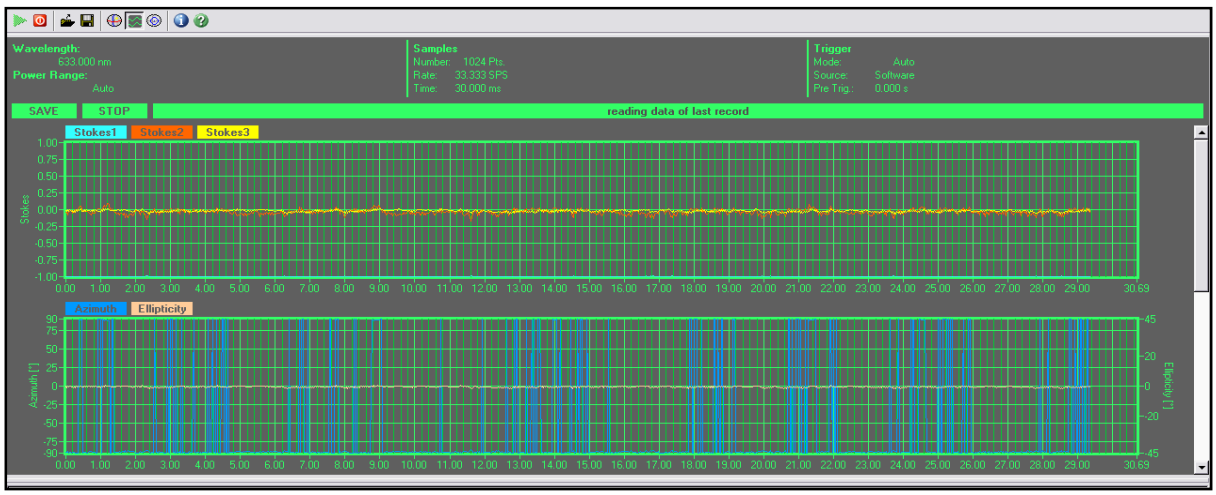

Figure 11: polarization state of plane polarized light with 0 deg azimuth represented by scope view of TXP polarimter software bundled with PAX 5710 VIS/NIR polarimeter

in H and none in V and thus would be horizontally polarized. The point P shown in the figure at which U and V axes intersect the sphere would similarly correspond to +45^{o} linear left hand circular polarization. Partially polarized signals can be represented by overlaying the poincare sphere with another sphere whose radius is the total signal power, I. The ration of the radii of the spheres is the degree of polarization p = I_P/I. The difference of the radii is thus the unpolarized power I_U = I-I_P [31]. From this we can add that by normalizing the total power I to unity, the inner, poincare' sphere has a radius P and will increase or decrease in diameter as the degree of polarization changes. The polarization state represented by a point P moves on the surface of the Poincare sphere with changing polarized part of the signal (Mott, 1986; McCormick and Hendry, 1985; Bebbington et al., 1987; Santalla et al., 1999).

Regarding the polarizers, the setup we have used consists of a linear polarizer followed by a quarter waveplate, then followed by another linear polarizer. The first linear polarizer is aligned to the lasers natural polarization to produce a beam with a polarization as close as possible to become perfectly linear. This is passed through a quarter wave plate aligned so that its first and slow axis is at 45^{o} to the incident beam's polarization. This produces a phase

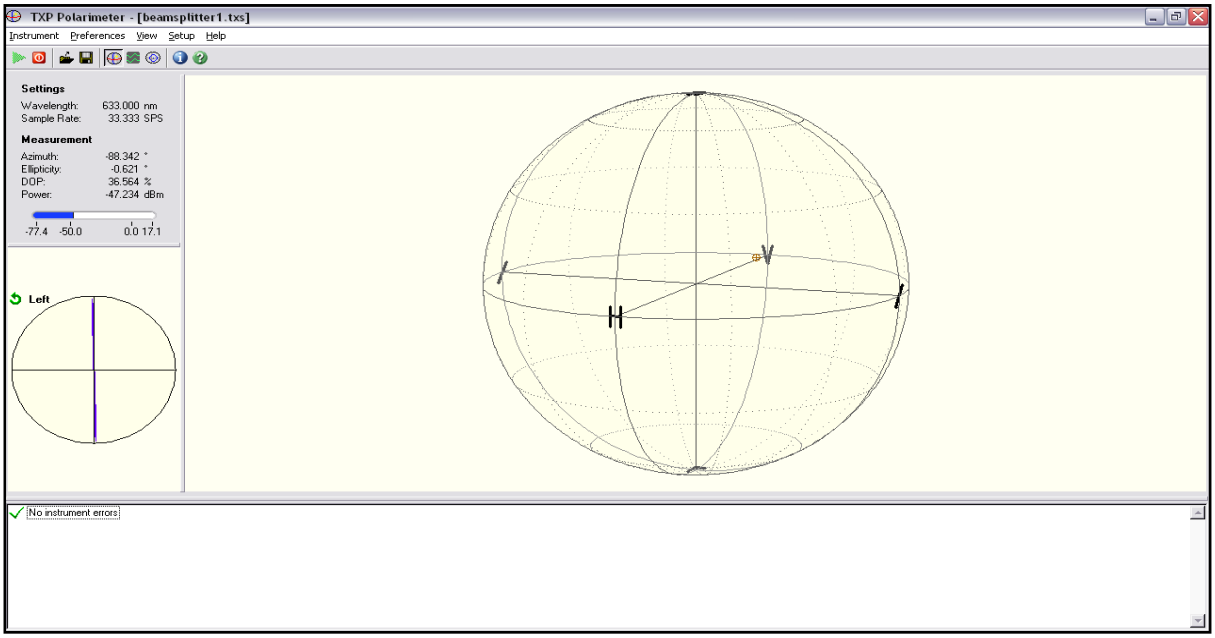

Figure 12: Poincare sphere representation of incident laser polarization through txpuser software(vertically linear polarization can be seen by the position of the red point

shift between the horizontally and vertically polarized components resulting in a beam with the polarization direction which rotates with time. As the two components entered the waveplate with equal intensity, the beam is converted to a circularly polarised beam by the waveplate. The second linear polarizer now converts the polarization of the beam back to linear but with the exception that now by rotating the final polarizer we can change the angle of polarization of the incident radiation without affecting the intensity of the beam. The final Poincare' sphere is shown in the fig- 11.

The polarizing filter assembly is easier to set up if we put one polarizer at a time while monitoring the output in the PC from the PAX polarimeter sensor head. At first the first

linear polarizer is placed in the path of the laser beam and then rotated with the dial to maximize the intensity of the beam which is monitored with the polarimeter software TXP server in the pc. The software calculates the power received by the sensor head in dBm with negative sign as it measures the power deterioration from 1 mW reference level. Next a quarter wave plate is placed after the linear polarizer and rotated slowly until we got a perfectly circularly polarized light beam with left handed rotation (noted by L in the Poincare' sphere representation). Finally another linear polarizer is placed after the wave plate as a final stage and it is noted that the beam is now perfectly linearly polarized and polarization angle can be changed without changing beam intensity. For our purpose at this moment we will use a horizontal linearly polarized beam (signified by point H in the poincare' sphere).

Previously it was shown that after the insertion of the ND 2.0 neutral density filter the power output should be around 0.01 percent of 5 mW He-Ne laser power. By power meter it is measured to be approx 60μW. From the polarimeter it can be seen that at desired H-polarised linear beam the power reading is -30.328 dBm. Now we know,

Transmitted power $P = 10\log_{10}(\frac{I}{Io})$ where I is the dissipated power in the polarizing stage and I_0 is the reference power level 1mW. From this equation we can get, I = 0.9267 μW, which suggests 1 μW power less than incident beam power to the polarizer assembly which was 60μW.

5.4 Laser line Filter:

We used a Semrock laser line filter [part number LL01-633-12.5] with 12.5 mm diameter to block off auxiliary laser lines generated by the 632.8 nm He-Ne laser. Semrock claims to have >90% transmission in the 2 nm bandwidth along 632.8 nm line. By calibrating the filter using a Hg-arc lamp white light source we observed that the spectral line bandwidth to be around 7 nm.

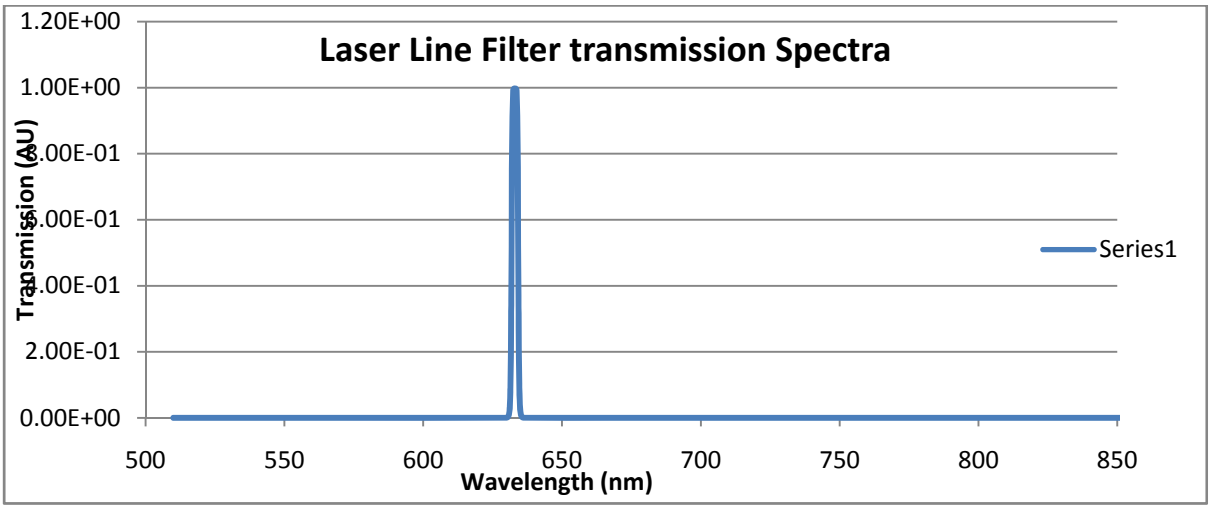

Figure 13: Laser line filter transmission spectra

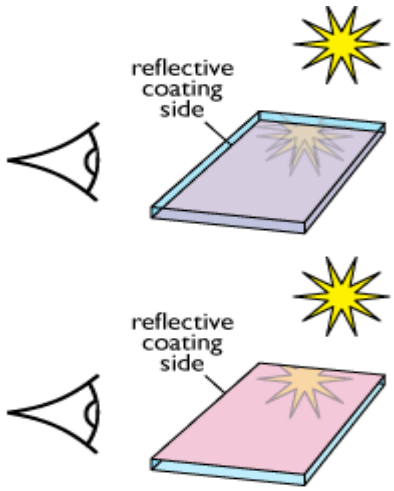

Figure 14: Reflective coating side determination by eye –pic courtesy [32]

5.5 Notch filter (Dichroic Mirror):

We used a dichoric mirror from Semrock [Part number-Di01-R635-25x36] to reflect 632.8-647.1 nm band and transmit 663.3-1200 nm band. We used plane polarized laser excitation as explained before so transmission and reflection efficiency was respectively 93% and 90% at 45^{o} angle of incidence. The mirror substrate is made of fused silica which helps reduce significant autofluorescence [32]. In our case the dichoric mirror was unmarked so when viewing the reflective coating side down, we can see the double reflection of the bright laser line and the thickness of the filter at the far edge is apparent. And when viewing the dichroic mirror with reflective coating side up, we can see the single reflection of the bright laser line and the thickness of the far edge of the filter is not visible. Thus the reflective coating side was marked and used as the incidence plane for the excitation laser. The dichroic mirror was mounted on a kinematic mount to properly align the mirror at 45^{o} to the angle of excitation laser incidence.

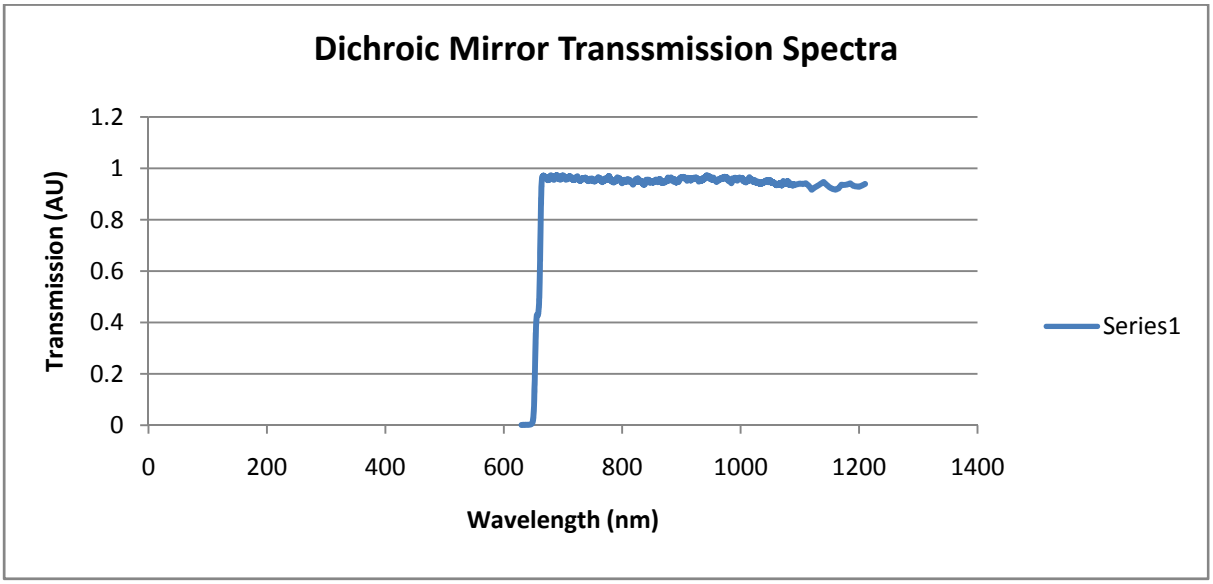

Figure 15: Dichoric Mirror Transmission spectra

5.6 Barrier Filter (Long Wave Pass Filter):

The long pass filter [part number-BLP01-635R-25] that have been used shows a laser blocking wavelength range of 632-642 nm and pass band of 660-1200 nm. The transition width from stopband to passband is approximately 16 nm. This LWP filter matches perfectly with the LL01-633-12.5 laser line filter that we have used. We have not used Razor-edge Raman filters [part number-LP02-633RE-25] with very low transition width and passband starting from 633.6 nm for cost reduction purposes [33]. Our long pass filter transmission band starts approximately from 660 nm which corresponds to approximately 500 cm^{-1}

wavenumber which indicates that raman shifts occurring below 500 cm^{-1} is absorbed by long pass filter. This is one of the reason that we could not identify the characteristic raman band at 487 cm^{-1} .

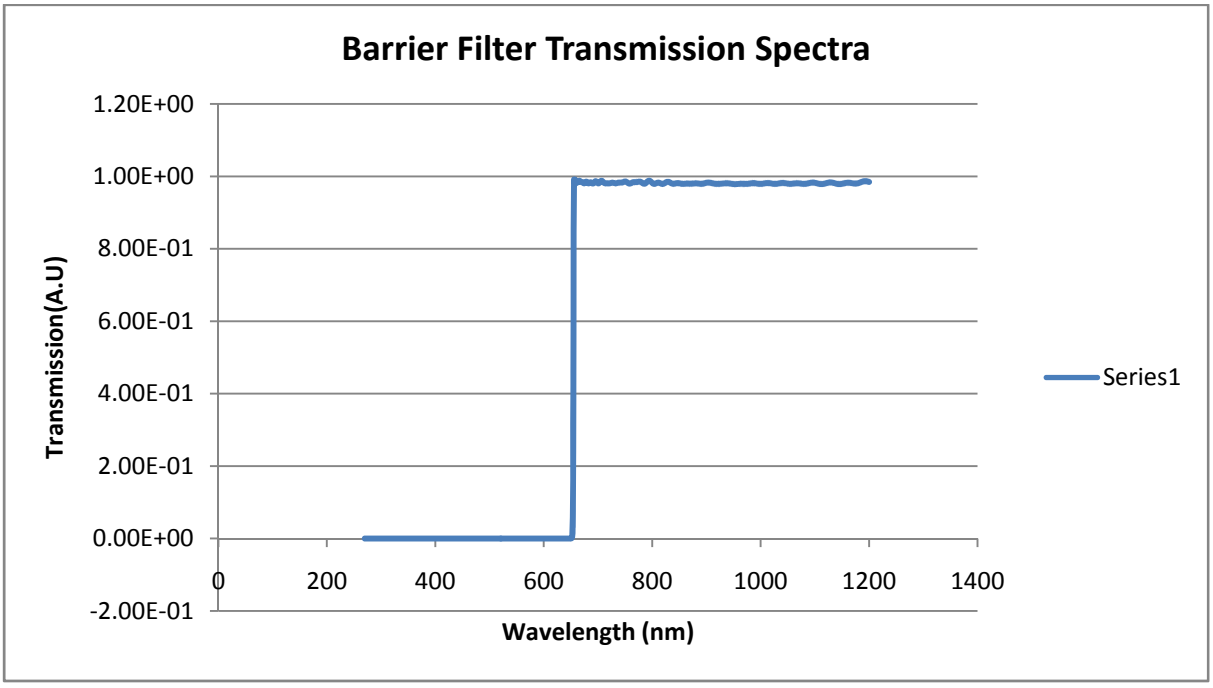

Figure 16: Barrier Filter transmission spectra

5.7 TP 300 RT VIS/NIR Fiber Probe:

Figure 17: TP 300 RT VIS/NIR transmission probe from ocean optics [pic-courtesy (34)]

We have used TP 300-RT transmission dip probes for weak Raman scatterers for coupling our HR-4000 modular spectrometer and light sources to measure the Raman scattering. These probes are very useful for embedding into process setup and properly aligning signal direction and light path in real-time monitoring [34]. These transmission dip probes transmit light from the illumination fiber through a plano-convex lens and through the sample compartment to a second surface mirror. The light reflects from this mirror and is focused by the lens onto the read fiber. Trade-off with these probes are that they have no inbuilt optics to discriminate backscattered excitation signal from the sample compartment and have internal reflections that limit the dynamic range of the measurement. Still the lucrative low cost of these probes make them an option for many on-line and lab applications.

5.8 CCD based Modular Spectrometer:

The HR-4000 Ocean optics spectrometer is a broadband UV/VIS/NIR spectrometer and can be equipped with 6 different slit sizes and 14 types of gratings [35]. However in our case the slit size was 5 µm and grating used was HC1. The resolution of the spectrometer depends on the slit size and grating. We used a 300µm diameter P300 VIS/NIR ocean optics fibre optic cable for collection purposes. There are several parameters important in determining the dispersion and optical resolution of a spectrometer. The most important of these are groove density, spectral range and blaze wavelength [35].

Groove density (mm^{-1}): It determines dispersion of the spectrometer which in turn defines the most efficient region of the spectrum. With increasing groove density of the grating, optical resolution increases but the spectral range of the spectrometer becomes more truncated.

Spectral Range: It determines the dispersion of gratings across the linear CCD arrays. It is also expressed as the "size" of the spectra on the array. The spectral range 'bandwidth' is a direct function of groove density and does not change. The wavelength range of a spectrometer is the sum of starting wavelength and spectral range. Higher the starting wavelength the more truncated the spectral range become.

Blaze wavelength: Gratings are fixed in the spectrometers unlike scanning monochromators to ensure long term stability and performance. Generally two types of gratings are used in spectrometers namely holographic gratings which reduce stray light perturbation and have a greater non-linearity correction and Ruled gratings which are highly sensitive and more reflective in the efficient region of the spectral range. Blaze wavelength in case of ruled gratings is the peak wavelength in an efficiency curve. For holographic gratings it is the most efficient wavelength region.

Best Efficiency (>30%): All ruled or holographically etched gratings optimize 1st order spectra at certain wavelength regions; the most efficient region is the range where efficiency is greater than 30%. Beyond the spectral range the wavelengths will have lower intensity due to the gratings reduced efficiency.

In our case we used grating HC1, a variable blazed grating with a broadband range which does not come with the package and had to be bought and installed separately.

Grating No	Intended Use	Groove Density	Spectral Range	Blaze Wavelength	Best Efficiency
HC1	UV-NIR	300mm^{-1}	200-1100 nm	variable	200-1100 nm

Optical Resolution:

To determine the optical resolution of the spectrometer at first we have to determine the dispersion of the spectrometer. Dispersion is defined by spectral range divided by number of detector elements in the CCD array of the spectrometer. Now from Ocean optics HR 4000 manual we can see that the spectral range for the HC-1 grating is 200-1100 nm. And the Toshiba CCD array that has been used in the spectrometer as detector has 3648 pixels as detector elements. So now dispersion is [36];

$$\text{Dispersion} = \frac{\text{Spectral Range}}{\text{No.of Detector Elements}}$$

Now for pixel resolution which depends on the slit size and from the spec sheet for HR 4000 spectrometer it can be seen that for 5 μm slit size the pixel resolution is 2.0 pixel. Optical resolution is given by multiplying the pixel resolution and the dispersion of the spectrometer. So after calculation we can find that for HC1 grating and 5 μm slit size HR 4000 modular ocean optics spectrometer displays a resolution 0.10-0.60 nm (FWHM).

Resolution could be further improved at the trade-off of sensitivity with the use of a finer grating which is available up to 1800 lines/mm groove density. If these finer gratings are used, it should be noted that the grating blaze wavelength must match the laser wavelength closely. The Ocean Optics HR 4000 spectrometer used to detect the Raman scattering uses a 3648 pixel CCD detector array. The CCD array behaves much like a photographic film in that the array integrates incident photons over time. Thus with longer exposure time, the detection of less intensified light is increased. Because Raman scattering is very weak and faint the integration time is set for about 55 s with averaging set for 30 exposures; so a single measurement takes about 7-9 mins.

6. Experimental Details:

The experimental setup consists of two different types of assembly as shown on fig – 16 and fig- 17 depending upon the sample type. In case of strong Raman scatterer like Klarite 307 SERS substrate coated with presence of Thiophenol, assembly -1 (shown in fig-16) was used which consists of extra dichoric mirror to prevent excitation line backscattering.

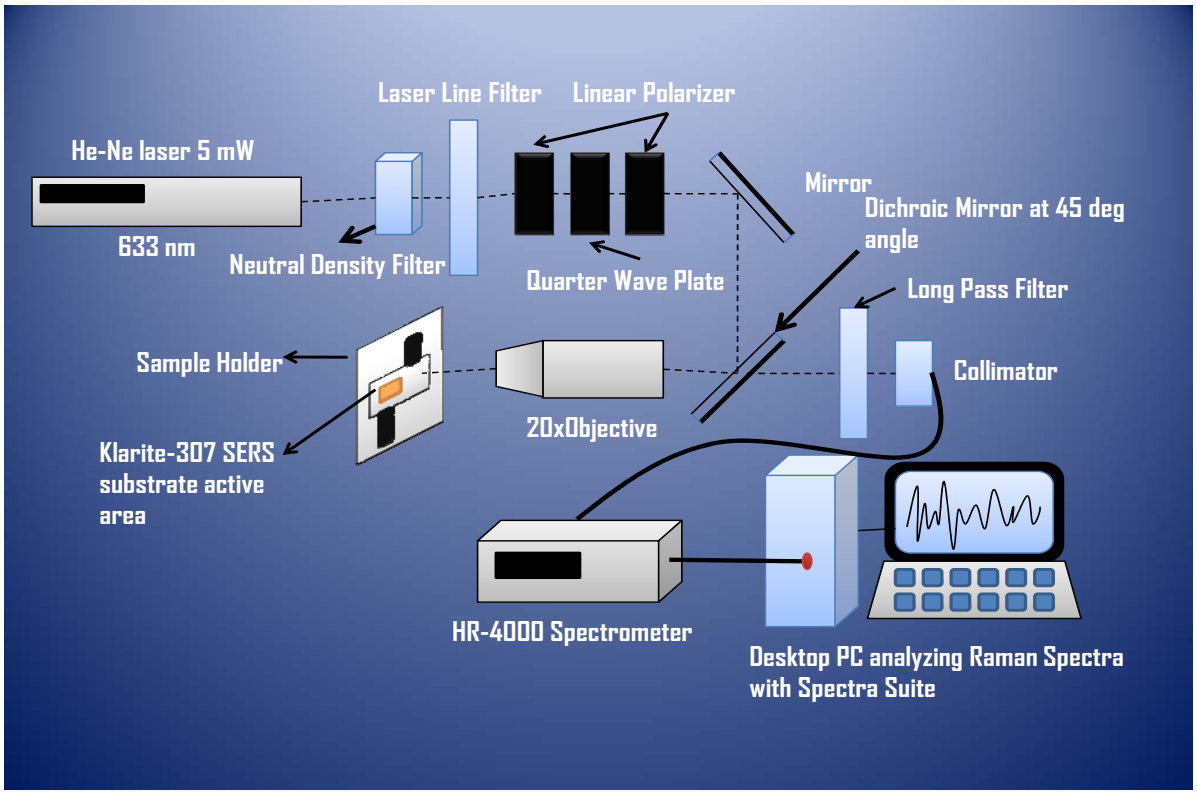

Figure 18: setup assembly schematics 1 used for detection of Raman bands from klarite-307 SERS substrate.

The beam from the 632.8 nm, 5mW linearly polarized laser is passed through a laser line filter from Semrock allowing only 632.8-633 nm line to go through. Then a mirror assembly was used to direct the beam to a 45^{o} angled with the incident laser dichoric mirror which acts as a notch filter and only reflects the 630-635 nm band and passes the rest of the spectral band. The reflected laser then focussed onto the sample klarite-307 fixed with the sample holder. Scattered raman signal is collected across the dichoric mirror and passed through a long wave pass filter. A collimator lens fixed on a detector mount then collects the invisible raman scattering and through a 400 µm diameter optical fiber passes it through a 5 µm slit of the HR-4000 modular spectrometer. The pc connected with the spectrometer then analyses the resultant spectra with the help of Ocean optics software spectrasuite which comes with the spectrometer. To observe polarisation effects, the polarization assembly consisting 2 linear polarizer and one quarter waveplate is placed between laser and sample with the help of polarimeter to ensure lowest power loss with required linear or circular polarization with appropriate azimuth angle. Due to use of the long wave pass filter edge of which starts from 650 nm translating into approx 500 cm-1 , any peaks or spectral lines below 500 cm-1 were absorbed by the LWP. The samples used in this experiment have large enough Raman shifts that peaks can be observed even without the use of dichoric mirror notch filter.

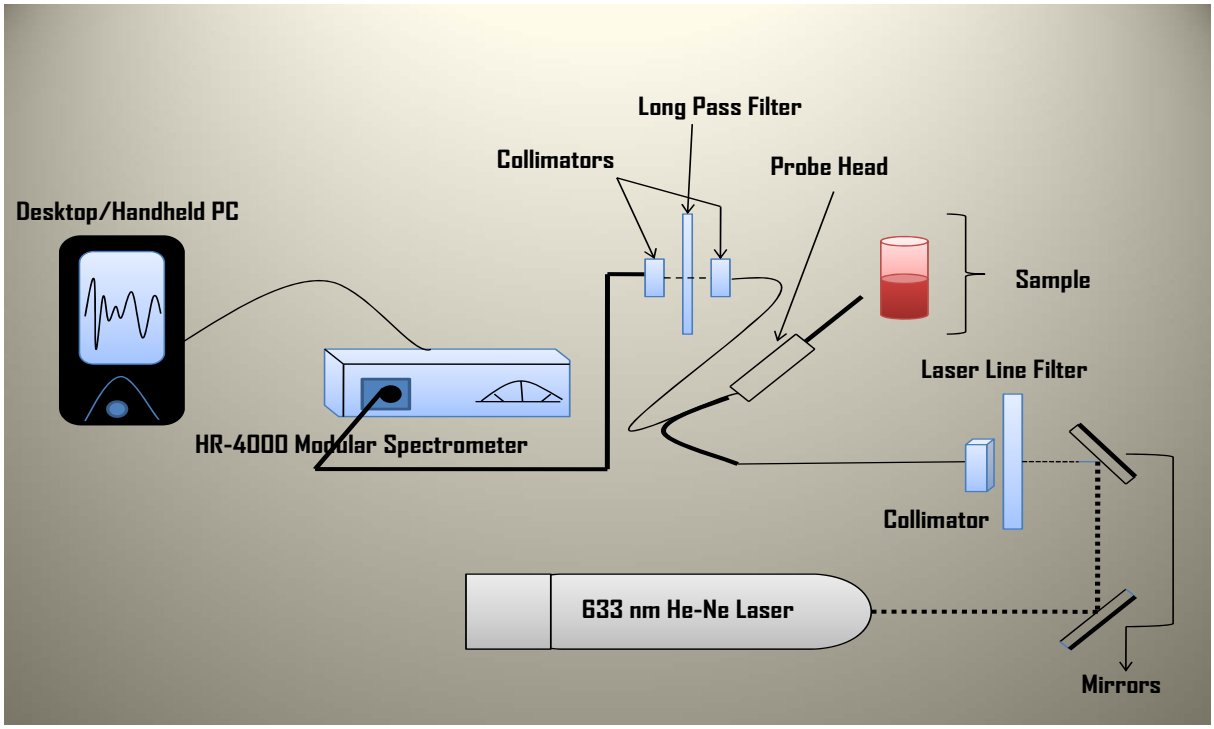

Figure 19: setup assembly schematics 2 used for detection of Raman bands from Isopropanol and commercial grade paracetemol

In case of liquid samples (2-Propanol) and relatively weaker raman scatterer samples like commercial Paracetemol a separate configuration was used consisting a fibre optic probe for focusing and collection optics. The light emitting from the read fibre lens of the TP-300 RT probe was passed through long wave pass filter to filter out the Rayleigh line and fixated to the spectrometer slit. An extra collimator lens was used in between the read fibre and the long wave pass filter for coupling purposes. The long wave pass filter BLP01 manufacturer, Semrock shows transmission band starting from 660 nm so in effect the long pass filter absorbs the anti stokes lines and transmit only the lower wavenumber stokes lines. The fibre optic patches to the spectrometer have a 400µm diameter. The whole experiment was conducted in dark in order to prevent room light and monitor screen light from reaching into the detector. The USB connected HR-4000 modular spectrometer is connected to a desktop pc. Ocean optics software spectrasuite is used to collect and process data. Reasonably satisfactory spectra were obtained from neat Isopropyl alcohol solutions, klarite-307 SERS substrate coated with Thiophenol, commercial grade Paracetamol. However for silicon wafer the main identifiable raman band of silicon which resides over 487 cm^{-1} could not be seen as it is well below our long wave pass filter absorption band. It is clear from the experiment that higher signal to noise ratio of the raman spectra can be obtained with higher power and more costlier lasers like 40-mW Ar^{+} ion laser which was also available in the lab. The ocean optics spectrometer software Spectrasuite allows integration times to be varied from 1ms to 65s which was adjusted from 40s-60s depending on the raman scattering ability of the samples. Electric dark correction was used to reduce background shift of the spectra. For most of the measurements more than 30 scans to average was used which made each measurement to take nearly 8-10 mins of time. Raman spectra's relative weakness in comparison to pixel noise and ghost pixels, which appears as sharp intense very low base width or baseless spikes

in the spectra, a dark measurement with laser light blocked corresponding to each measurements must be taken and duly subtracted from the measurement spectra. After the dark spectrum subtraction which is explicitly available in the ocean optics interfacing software, Spectrasuite the spreadsheet data is exported to custom built software named SWizard, by S.I Gorelsky, University of Ottawa [37]. This software facilitates savitsky golay polynomial smoothing algorithm and takes lorenzian of the prominent raman bands. This post processing technique was applied to retrieve characteristic raman bands from the noisy spectra. Due to reasonably low power of the laser and high integration time formidable amount of background noise was picked up by the HR-4000 spectrometer. As scaling factors were introduced in the resultant data as required, therefore, relative intensities of peaks are not quantitative. Raman scattering intensities were collected as unitless channel counts.

7. Results and Discussion:

As explained before experimental Raman spectroscopy has traditionally been a very expensive endeavour. Besides being costly, the large components have significantly lowered the portability of a traditional Raman analysing system. From Fig-2 and fig- 16 and 17 we can depict a relative setup schematic comparison between tradition and our miniaturized, lower cost Raman setup. Table- 3 also provides and summarizes the approximate cost, size etc. of the components for both the conventional and miniature, simplified Raman instruments.

Table 3: Comparison between conventional and miniature simplified Raman spectrometer setup in terms of cost, dimensions etc

Component	Cost (Pounds)	Size (Cm)	Weight(Kg)	Manufacturer	Model No.
Standard					
Ion Laser	30,000	150x25x25	45	Spectra physics	2060
Optics	117	10x6	0.3	Edmund	
Notch filter	528	2.5x35	0.9	Semrock	NF01-532U-25
Spectrograph	8850	55x40x40	23	Acton	VM-505
CCD	20000	20x10x5	2	Roper scientific	Spec-10:400B
Computer	354	50x50x20	4	Dell	-
Monitor	60	30x30x20	9	Dell	-
Total	60000	250810 cm^{-3}	83.4	-	
Miniature					
Laser	687	45x5	5	ThorLabs	HRP050
Fibre Probe	513	1000x0.5	0.1	Ocean Optics	TP-300 VIS/NIR
Laser Line filter	174	12.5 mm	0.5	Semrock	LL01-633-12.5
Dichroic Mirror	115	25 mm	0.5	Semrock	Di01-R635-25x36
Long-Pass filter	174	12.5 mm	0.5	Semrock	BLP01-635R-25
Spectrometer	2750	15x11x5	1.5	Ocean Optics	HR-4000CG VIS/NIR

CCD	-	Inbuilt		-	Inbuilt
Desktop Pc	600	50x50x20	13	Compaq	-
Total	5013	1515 cm^{-3}	22		

It is a rough estimate of the cost based on the systems available in the lab and used in the setup. Readily available and cheaper counterparts of traditional expensive Raman systems have been used to demonstrate the feasibility of performing measurements on some strong Raman scatterers and SERS substrates with a small and inexpensive setup. Obviously, conventional setups have many advantages like wavelength selection, more power, higher sensitivity and higher resolution over the presented low cost prototype. However for demonstration and simple measurement and analytic purposes this approach is an attractive alternative. The significant cost and space savings along with portability offsets the compromises with resolution and sensitivity. Fig-16 shows the applicability of the 632.8 nm He-Ne 5 mW laser as an excitation source for resonant molecules coated on SERS substrates as well as commercial strong raman scatterers. Thiophenol is resonant at 650 nm and starts showing pre-resonance enhancement at 633 nm. Other samples like neat Isopropyl alcohol and commercial grade Paracetemol tablet are not resonant at used excitation wavelength. Fig-20 shows high quality post-processed SERRS spectra of thiophenol coated on gold colloid acquired using 633 nm He-Ne laser as excitation source. The spectrum in general shows clear and well defined peaks characteristics of Thiophenol on gold colloids SERS substrate. Measurements have been taken with 50 sec integration time and 30 scans to average with detector non-linearity correction and electric dark correction checked on in the Spectrasuite bundled software of the HR-4000CG modular spectrometer. Dark spectrum and reference spectrum is taken and the resultant spectrum data is gathered after the duly subtraction from the dark spectra. For post processing purposes the resultant spectrum data is exported to excel and converted to freeform .log format. The .log file is then imported into a spectra processing free software named SWizard, made by S.I Gorelsky of University of Ottawa to employ Savitsky-Golay smoothing which is basically a local polynomial regression on a distribution to determine the smoothed value for each point, Lorentzian curve fitting and scaling factors [37]. The resultant data is generated by convoluting peaks with Lorenzian curves and plotting into GNU Plot. In our case we have imported the data into Excel again and generated the final Raman spectra. As explained before the bands below 500 cm^{-1} is absorbed by the long pass filter because of the transmission spectra of LWP filter starting from 660 nm. Benzine ring presence in Thiophenol is clearly seen from the 1001 cm^{-1} line. Peaks at 1141 cm^{-1} did not resolve properly due to 10 cm-1 resolution of the setup and appear to be one peak with broad peak base rather than 3 distinct peaks. Peaks on the far side of 3000 cm-1 is supposedly chopped off by fused silica glass element used in many of the filters and collimating lenses and thus cannot be seen. This effectively reduced the resultant working Raman spectra band of out setup to 500-3000 cm-1. Some extraneous broad raman peaks generated by the objective, collimating lenses coating and fiber optic patches are removed by background substraction since they are constant in a given excitation power.

Frequency(wavenumbers) cm^{-1}	Vibration	Compounds
624	ring deformation	mono-substituted benzines
701	CS stretch	alkyl sulfides
929	trigonal ring breathing	mono-substituted benzines
1002	trigonal ring breathing	mono-substituted benzines
1038	In plane CH deformation	mono-substituted benzines
1584	ring stretches (doublet)	benzine derivative
2580	SH stretch	Thiols

Table 4: raman vibrational band shifts and corresponding bond vibrations in Klarite-307 substrate confirms Thiophenol presence

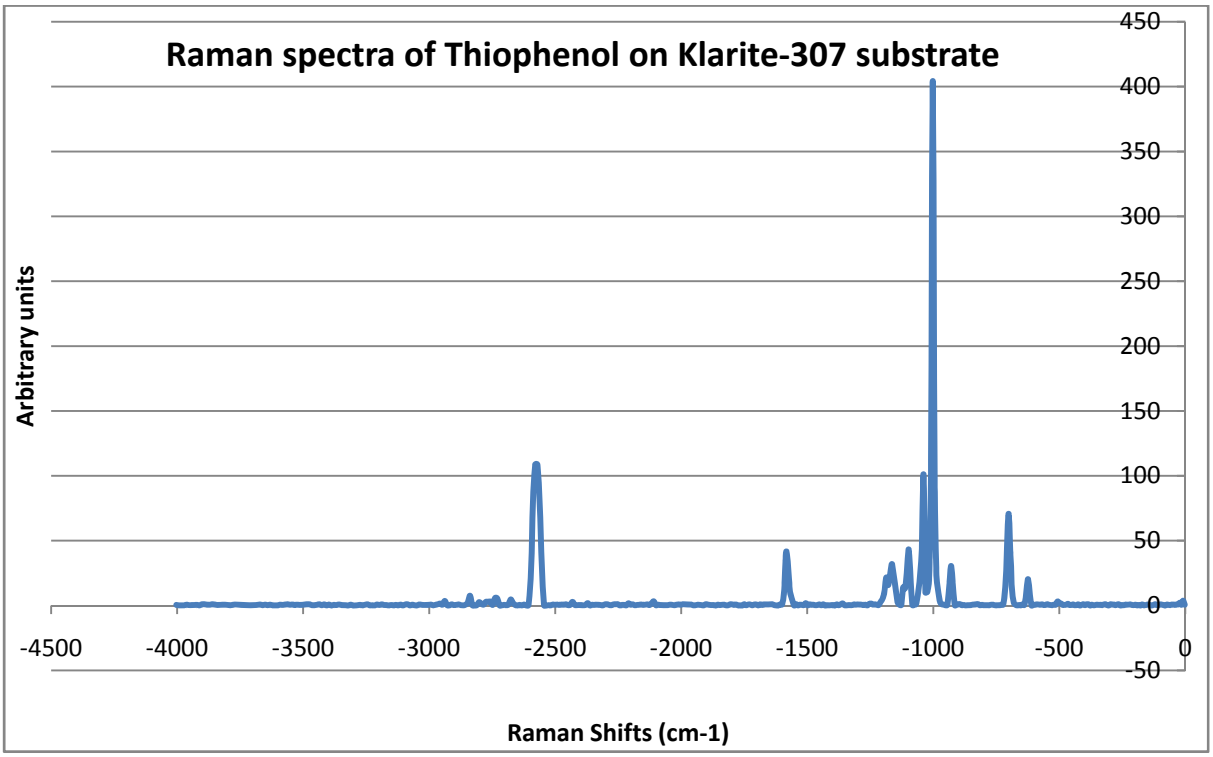

Figure 20: Raman shifts for Klarite-307 substrate demonstrating mono substituted benzine and thiol group presence.

A second setup was conducted to increase incidence power on the sample for relatively weak Raman scatterers by altering the collection optics and light delivery of the system. Fig- show the case where the light delivery, focusing and collection optics are replaced by a TP-300 RT VIS/NIR fiber optic transmission probe. The light was delivered from the 633 nm He-Ne laser to the sample through the probe and the scattered light was collected by the probe and focused onto a collimator lense which then in turn after passing through a long pass filter focused into the slit of the HR-4000 spectrometer by another collimator lens. In case of isopropanol measurement the spectra generated by the empty sample case illuminated by the excitation laser is taken to as reference spectra to subtract the background extraneous raman vibrations generated by the polyethylene plastic container. A flat mirror from ocean optics mounted on a post and holder was placed behind the transparent isopropanol sample in the container to reflect back the scattered light and focused into the transmission probe reading head. In the resultant spectra bands at 453 cm^{-1} and 387 cm^{-1} are not present and the 480 cm-1 band possesses a sharp falling edge. This again explains the presence of the 660 nm transmission band long pass filter which absorbed bands below 500 cm^{-1} approximately. The peak at 1110 cm-1 did not resolve because of the 11 cm-1 resolution of the HR-4000 spectrometer and converted the 1142 cm-1 peak into a broader base. The peak at 1350 cm-1 did not showed in the spectra and a 2757 cm-1 weak band corresponding to OH-bond of isopropanol resolved only. The far side shifts from 2800 cm-1 onwards were chopped off by the extensive use of fused silica glass materials and components which absorbs and chops off signals above 2 micron approximately [38]. Placing the polarizer assembly set with both horizontal and vertical linear polarization in front of the sample denigrates the raman spectral band intensity. OH bond raman band vanishes along with 958/980 cm-1 band. Peak to peak and peak base width ratio compared with Sigma-aldrich FT-NIR raman vary by only 5% in our resultant spectra.

Frequency(wavenumbers) cm^{-1}	Vibration	Compounds
850	skeletal stretch	Isopropyl group
1452	CH deformation	Isopropyl group
2775	0-H stretch	OH bond

Table 5: Isopropanol raman shifts and corresponding characteristic bond vibrations

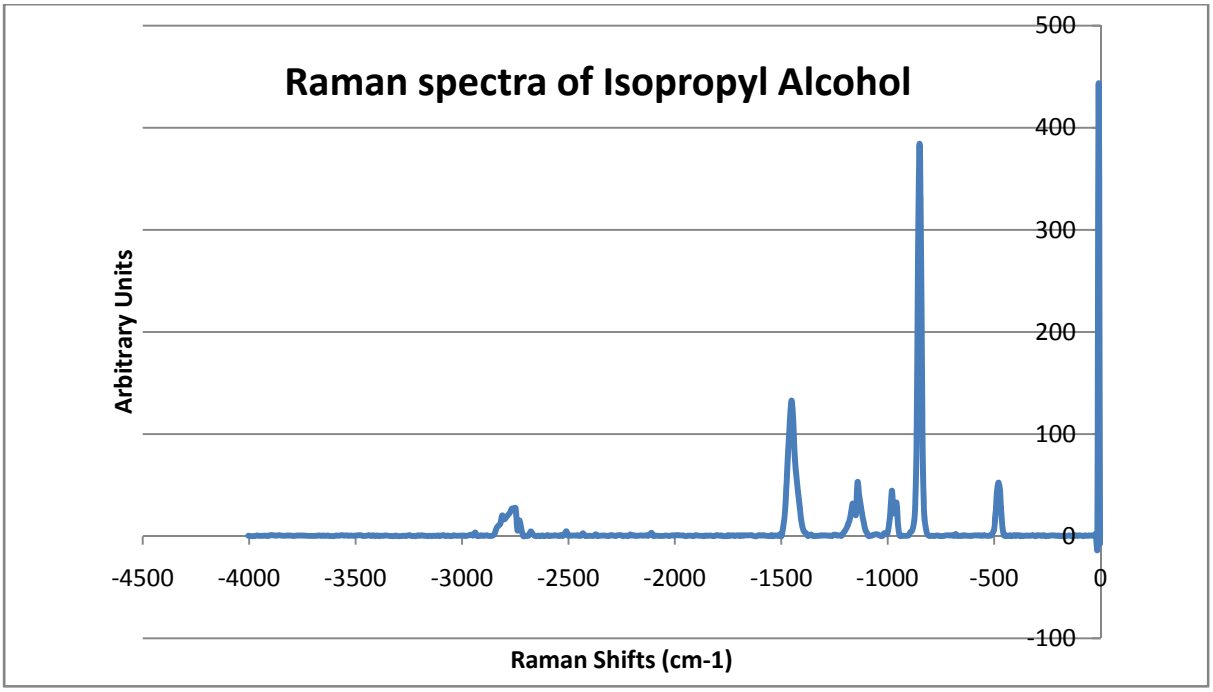

Figure 21: Raman spectra of isopropanol displaying characteristic isopropyl group C-H stretch and weak O-H bond vibrations

In case of commercial grade paracetamol [para-acetylaminophenol] sample to get a satisfactory spectrum the tablet had to be thoroughly cleaned and the surface was intentionally roughened and a groove has been made on the surface. The results from the spectra it is seen that generally this tablet was very homogenous. However the Gaussian laser beam spot size for analysis was too large to detect the minute component difference of the paracetamol tablet [39]. Raman spectroscopy alone should not be used exclusively in this kind of measurement to detect component and ingredient distribution. IR, FT-IR and UV spectroscopy often compliment Raman spectroscopy as each method is sensitive to different components of a sample. Raman spectroscopy is more sensitive to vibrations from C=C bonds whereas IR spectroscopy is keener on detecting vibrations resulting from polar bonds such as O-H bonds [39].

Table 6: Paracetemol raman shifts and corresponding characteristic bond vibrations

Frequency(wavenumbers) cm^{-1}	Vibration	Compounds
1576	ring stretches(doublet)	benzine derivatives
1607	NO_2 scissors	primary amides
1647	NO_2 scissors	primary amides

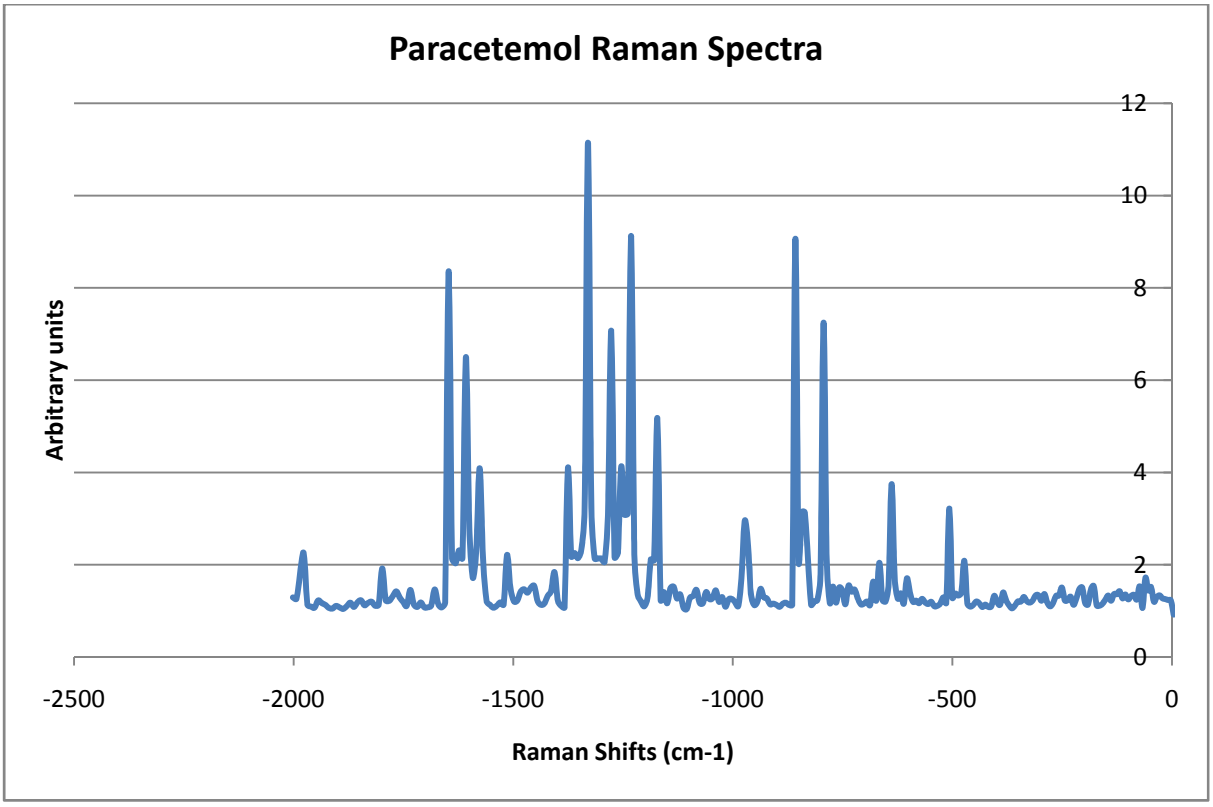

Figure 22: Raman spectra of Paracetemol displaying characteristic of primary amines and benzine derivatives

The resultant spectras compare quite favourably with the published spectral data. While there is much room for improvement, this demonstration of acquiring significant raman spectras utilizing low power and low resolution setup is significant. This represents a considerable step towards the miniaturization of Normal raman and SERRS instrumentation.

8. Conclusion:

A low cost, low power 633 nm He-Ne laser based optical benchtop raman spectrometer for demonstrational purposes has been assembled. The instrument does not perform like a research grade instrument, but regardlessly it can be used to extract stokes bands for compounds such as Isopropyl alcohol, paracetamol or SERS substrates such as Klarite -307 and make depolarization ratio measurements. The open architecture of the spectrometer gives the user a greater insight into raman spectroscopy that can be achieved in “dry lab” exercises. The low cost and simplicity of construction of the instrument offers a practical alternative for the demonstration of Raman spectroscopy.

Bibliography:

1] ***Analytical Applications of Raman Spectroscopy;*** Pelletier, M.J., Ed.; Blackwell: Oxford, 1999.
2] Chase, B. ***A new generation of Raman instrumentation***. Appl. Spectrosc. 1994, 48 (7), 14A–19A.
3] Lewis, I. R.; Griffiths, P. R. ***Raman spectrometry with fiber-optic sampling***. Appl. Spectrosc. 1996, 50 (10), 12A–30A.
4] Atkins, P.; de Paula, J. ***Physical Chemistry, 7th ed***.; Freeman: New York, NY, 2002.
5] ***Nobel Lectures (Physics),*** 1922-1941. New York: Elsevier Publishing Company, 1965, 263-277
6] National Historical Landmarks, American Chemical Society, taken on 10th September, 2008, web resource: http://preview.interlockingmedia.com/acslandmarks/landmarks/raman/raman.html
7] J P Blond and D M Boggett, ***A simple Raman spectrometer***
8] Elumalai, P., Atkins, P., de Paula, J. *Atkins'* ***Physical Chemistry***, Oxford University Press, 2002
9] Rolf Bombach***, Application of Raman spectroscopy: Species concentration and temperature measurements for catalytically stabilized combustion,*** Paul Scherrer Institut, Switzerland, March 2002, Zurich
10] ***A Review of the Theory and Application of Coherent Anti-Stokes Raman Spectroscopy (CARS)*** Applied Spectroscopy, Volume 31, Number 4, July/August 1977, pp. 253-271(19)
11] P.R. Carey, ***Biological Applications of Raman and Resonance Raman Spectroscopies***, Academic Press, New York, p. 71, 1982.
12] ***Raman spectroscopy: a complex technology moving from lab to the clinic — and before too long, the marketplace***; retrieved on 10th September, 2008 web resource: http://www.opticsreport.com/content/article.php?article_id=1018&page=1
13] ***The Raman Effect: A Unified Treatment of the Theory of Raman Scattering by Molecules***, Derek Albert Long, published by John Wiley and Sons, 2002, pp-41-45
14] ***Fundamentals Of Molecular Spectrscopy***, Colin N. Barnwell, Elaine M. McCash, Published by McGraw Hill Companies, pp 100-107
15] ***Organic Spectroscopy***, L. D. S. Yadav, Published by Springer, 2005,pp-117-119
16] Fleischmann, M.; PJ Hendra and AJ McQuillan (15 May 1974). "***Raman Spectra of Pyridine Adsorbed at a Silver Electrode"***. *Chemical Physics Letters* 26 (2): 163–166.
17] Jeanmaire, David L.; Richard P. van Duyne (1977). ***"Surface Raman Electrochemistry Part I. Heterocyclic, Aromatic and Aliphatic Amines Adsorbed on the Anodized Silver Electrode"***. *Journal of Electroanalytical Chemistry* 84: 1–20. Elsevier Sequouia S.A..
18] Albrecht, M. Grant; J. Alan Creighton (1977). "***Anomalously Intense Raman Spectra of Pyridine at a Silver Electrode"***. *Journal of the American Chemical Society* 99: 5215–5219.
19] L. H. Qian, X. Q. Yan, T. Fujita, A. Inoue, and M. W. Chen, ***Surface enhanced Raman scattering of nanoporous gold: Smaller pore sizes stronger enhancements,*** Appl. Phys. Lett. **90**, 153120 (2007);
20] K.L. Davis, K.L. Liu, M. Lanan, and M.D. Morris, *Anal. Chem.* 65, 293 (1993).
21] P.C. Lee and D. Meisel, *J. Phys. Chem.* 86, 3391 (1982).
22] P.C. Painter and J.L. Koenig, ***Biopolymers*** 15, 2155 (1976)

23] L. Jensen , L. L. Zhao, J. Autschbach, G. C. Schatz, ***Theory and method for calculating resonance Raman scattering from resonance polarizability derivatives,*** J. Chem. Phys. **123**, 174110 (2005)
24] ***An Introduction to Biomedical Optics,*** Robert Splinter, Brett A. Hooper, Published by CRC Press, 2007, pp-273-276
25] ***Raman Spectroscopy application Notes***, Renishaw systems, web resource: http://www.renishaw.com/en/6259.aspx
26] Fetterolf, M. L.; Goldsmith, J. G. *J. Chem. Educ.* 1999, *76,* 1276–1277.
27] Benjamin A. DeGraff, Mandy Hennip, Julie M. Jones, Carl Salter, and Stephanie A. Schaertel, ***An Inexpensive Laser Raman Spectrometer Based on CCD Detection***, *The Chemical Educator,* Vol. 7, No. 1, Published on Web 02/01/2002
28] Vickers, T. J.; Pecha, J.; Mann, C. K. *J. Chem. Educ.* 2001, *78,* 1674–1675.
29] ***HRP 050 5mW He-Ne Laser product Catalogue*** THORLABS web resourcce: http://www.thorlabs.com/thorProduct.cfm?partNumber=HRP050
30] ***Neutral Density Filter Catalogue, Thorlabs***, web resource: http://www.thorlabs.com/NewGroupPage9.cfm?ObjectGroup_ID=266
31]***Degree of Polarization vs Poincare' Sphere Coverage-Which is Necessary to Measure PDL Accurately?*** White paper from ILX Lightwave, Laser diode Instrumentation and test Systems
32] ***Dichroic Notch filter catalogue Sheet***, Semrock, Web resource: http://www.semrock.com/Catalog/BrightLine_LaserMicroscopy_CommonSpecs.htm
33] ***Edge basic Long pass filter catalogue***, Semrock, web resource: http://www.semrock.com/Catalog/EdgeBasicLWP_spectra.htm#635
34] ***T300-RT VIS/NIR transmission probe catalogue***, Ocean optics, web resource: http://www.oceanoptics.com/products/t300t200transdipprobes.asp
35] Ocean Optics, Inc. http://www.oceanoptics.com/technical/ opticalresolution.asp (accessed Feb 2006)
36] ***HR-4000 Modular Spectrometer, Installation and Operation Manual***, Ocean Optics
37] SWIZARD manual, Serge Gorelsky, University of Ottawa, web resource: http://www.sg-chem.net/swizard/
38] Araujo et al., "***Absorption in Silica—A preliminary Model,***" Proceedings of SPIE—Inorganic Optical Materials, vol. 3424, 1998, pp. 1-7
39] ***Particulate Study of Paracetamol Tablets During Compaction***, Paul Martell, Department of chemical Engineering, University of Queensland
40] **IR/Raman spectra were calculated using the SWizard program**
S. I. Gorelsky, *SWizard program*, http://www.sg-chem.net/, CCRI, University Of Ottawa, Ottawa, Canada, 2008
41] Fiona C.Thorley, Kurt J. Baldwin, David C. lee, David N. Batchelder; **Dependence of The Raman spectra of Drug Substances upon Laser Excitation wavelength**; Journal of Raman Spectroscopy, J.raman Spectrosc. 2006; 37:335-341
42] **Combined Raman and FT-IR spectroscopy using IlluminatIR module for Renishaws inVia Raman microscopes**; Application Note from the Spectroscopy Products Division, SPD/AN/101 Issue 1.0 April 2004, Renishaw Systems
43] Lin-Vien, D; Colthup, N.B; fateley, W.B and Graselli, J.G. **The Handbook of Infrared and Raman Characteristic Frequencies of Organic Molecules.** Academic Press: Boston, 1991.